

# Magnetic field influence on the Néel, dimer, and spin-liquid states of the low-dimensional antiferromagnets $\text{NiTa}_2\text{O}_6$ and $\text{CoSb}_2\text{O}_6$

A. B. Christian, S. H. Masunaga, A. T. Schye, A. Rebello, and J. J. Neumeier  
*Physics Department, Montana State University, Bozeman, Montana 59717-3840, USA*

Yi-Kuo Yu

*National Center for Biotechnology Information, 8600 Rockville Pike, Bethesda, Maryland 20894, USA*

(Received 12 June 2014; revised manuscript received 14 October 2014; published 29 December 2014)

Magnetic susceptibility and heat capacity measurements are used to infer information about the short-range magnetic order above the Néel temperature  $T_N$  and the antiferromagnetically ordered states below  $T_N$  of quasi-one-dimensional (quasi-1D)  $\text{CuSb}_2\text{O}_6$ ,  $\text{NiTa}_2\text{O}_6$ , and  $\text{CoSb}_2\text{O}_6$ . It is shown that two antiferromagnetic sublattices, oriented at  $90^\circ$  to one another, are likely present in  $\text{NiTa}_2\text{O}_6$  and  $\text{CoSb}_2\text{O}_6$ . Application of magnet field parallel to the quasi-1D chains of one sublattice is perpendicular to the chains of the other sublattice. This results in two antiferromagnetic transitions when the magnetic field  $H \geq 2$  T ( $\sim 0.2$  meV). The anisotropic influence of magnetic field on the antiferromagnetic state leads to a magnetocaloric effect that is fully investigated in this work. The effect is associated with competition among Néel, dimer, and spin-liquid states that are all present at  $T_N$ .

DOI: [10.1103/PhysRevB.90.224423](https://doi.org/10.1103/PhysRevB.90.224423)

PACS number(s): 75.40.-s, 75.30.Gw, 75.25.-j, 75.30.Sg

## I. INTRODUCTION

Transition-metal oxides exhibit a wide range of interesting electrical and magnetic properties. Among these,  $M\text{Sb}_2\text{O}_6$  and  $M\text{Ta}_2\text{O}_6$ , where  $M$  is a transition-metal ion, display antiferromagnetism with reduced dimensionality [1–12]. Their Néel temperatures  $T_N$  are near 10 K, but short-range magnetic order [7,9,10,13] is evident well above  $T_N$ . In this region, broad peaks in their magnetic susceptibilities are indicative of one-dimensional (1D) order of magnetic moments on 1D chains. The short-range nature of the order in this region is suggested by other measurements such as Mössbauer spectroscopy [1] and heat capacity [2,9]. Below  $T_N$ , the 1D chains align to form three-dimensional order, sometimes exhibiting an energy gap [9,13]. The coupling between the 1D antiferromagnetic chains is weak [9,14,15], which invites classification as quasi-1D antiferromagnets.

One-dimensional antiferromagnetic chains are a category of Luttinger liquids [16]. Normally, long-range order is not expected for a 1D chain of magnetic ions. However, they can undergo phase transitions (i.e., dimerization, or a spin-Peierls transition) through coupling with 3D phonons [17,18]. Competition between nearest- and next-nearest-neighbor exchange energies ( $J_1$  and  $J_2$ , respectively) is known to lead to spontaneous dimerization if the relationship between them is favorable [19]. Furthermore, in the anisotropic  $XXZ$  Heisenberg model, a triple point, where Néel, dimer, and spin-fluid states of matter intersect, can arise depending on the ratio between  $J_1/J_2$  and the anisotropy parameter  $\Delta$  [19].

Real magnetic systems always possess interchain coupling. It is believed that this coupling can lead to long-range order [20–22]. For example, the quasi-1D antiferromagnet  $\text{Cs}_2\text{CoCl}_4$  possesses a coupling ratio [23,24] of  $J/J_\perp \sim 68$ ,  $\Delta \sim 0.25$ , and a Néel temperature of 0.22 K, where  $J$  is the coupling along and  $J_\perp$  is the coupling perpendicular to the chain. Magnetic field applied perpendicular to the chains breaks the symmetry, initially inducing a spin-flop phase, but

eventually it suppress long-range order leading to quantum fluctuations, and a spin-liquid phase emerges. The *spin-liquid* phase, lacking long-range magnetic order but exhibiting short-range order, is a magnetically frustrated system, unlike the *spin-fluid* phase, which is a gapless Luttinger liquid state [19] associated with a purely-1D system where  $|\Delta| < 1$ . Direct comparison of experimental observations in quasi-1D systems to theory for purely 1D is tenuous, and the theoretical complexity of adding interchain coupling requires a mean-field treatment. Such theoretical work has considered the quasi-1D antiferromagnet in magnetic field, suggesting that field perpendicular to the magnetic chain suppresses long-range order and induces the spin-liquid phase [24,25]. This type of field-induced phase competition is the subject of the present investigation. The present study differs from other studies of the influence of magnetic field on quasi-1D spin-chain systems, where field causes magnetization plateaus that are associated with the formation of triplet states [23,25]. No magnetization plateaus are revealed here, possibly because of complexities in the crystal/magnetic structure.

This work focuses on three of these compounds,  $\text{CuSb}_2\text{O}_6$ ,  $\text{NiTa}_2\text{O}_6$ , and  $\text{CoSb}_2\text{O}_6$ .  $\text{CuSb}_2\text{O}_6$  orders antiferromagnetically at Néel temperature [3,9]  $T_N = 8.5$  K,  $\text{NiTa}_2\text{O}_6$  orders [10,15,26] at  $T_N = 10.5$  K, and  $\text{CoSb}_2\text{O}_6$  orders at [8,13]  $T_N = 13.5$  K. They possess similar crystal structures, with the transition-metal  $M^{2+}$  ion residing in an octahedral environment.  $\text{CuSb}_2\text{O}_6$  undergoes a structural transition on cooling below 380 K from trirutile tetragonal ( $\alpha$ - $\text{CuSb}_2\text{O}_6$ ) to distorted monoclinic ( $\beta$ - $\text{CuSb}_2\text{O}_6$ ) while maintaining the octahedral environment [27].  $\text{NiTa}_2\text{O}_6$  and  $\text{CoSb}_2\text{O}_6$  possess the same tetragonal space group ( $P4_2/mnm$ ); the  $c$  lattice parameter of the unit cell is roughly double the  $a$  lattice parameter [8,26]. The crystal structure for these compounds is shown in Fig. 1; multiple unit cells and two  $M\text{-O}_6$  octahedra are shown to illustrate the fact that the apexes of the octahedra point along the  $[110]$  direction at  $z = 0$  and the  $[\bar{1}\bar{1}0]$  direction at  $z = 1/2$ . The oxygen occupancy does not allow the apexes to point along

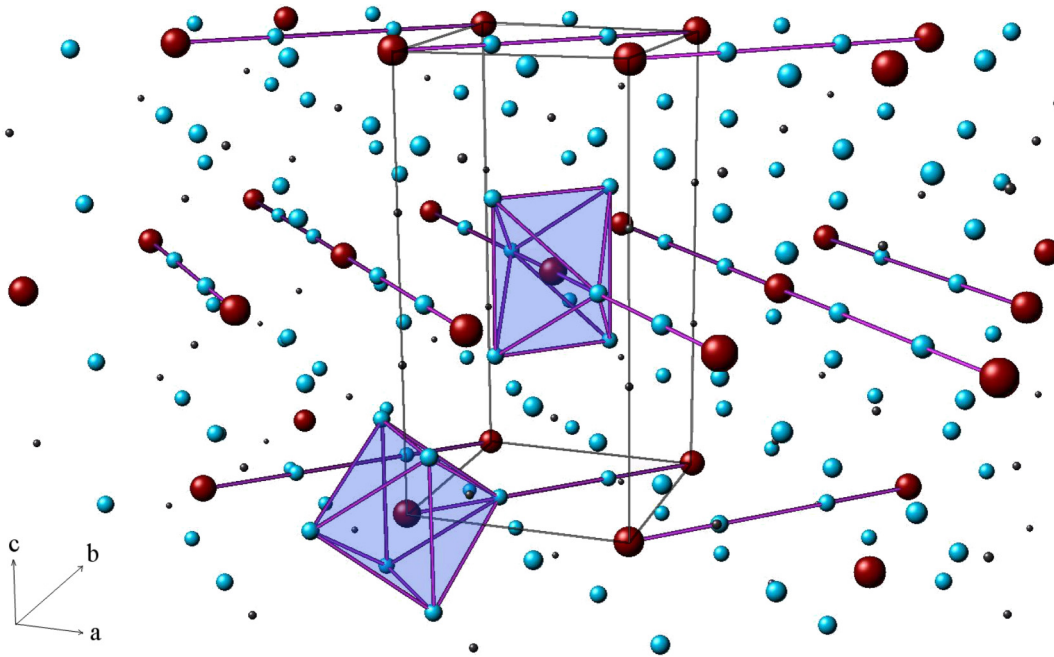


FIG. 1. (Color online) Tetragonal  $P4_2/mmm$  crystal structure for  $\text{NiTa}_2\text{O}_6$  and  $\text{CoSb}_2\text{O}_6$ . Except for the monoclinic distortion, this structure is valid for  $\text{CuSb}_2\text{O}_6$ . The  $M$  atoms are red, oxygen atoms are blue, and Sb or Ta atoms, reduced in size for clarity, are gray. The unit cell is illustrated by thin lines. The one-dimensional  $M$ -O-O- $M$  linkages along the  $[110]$  and  $[1\bar{1}0]$  directions at  $z = 0$  and  $z = 1/2$ , respectively, are illustrated by lines. One octahedron is shown for each layer; the apexes of the octahedra form the  $M$ -O-O- $M$  linkages, which can *only* point along  $[110]$  and  $[1\bar{1}0]$  at  $z = 0$  and  $z = 1/2$ , respectively. The four in-plaquette  $M$ -O bond distances are 2.0683 Å, the two out-of-plaquette bond distances are 2.0265 Å, and the octahedra apexes are separated by 2.5223 Å in the case of  $\text{CoSb}_2\text{O}_6$ . Java Structure Viewer was used to create this figure.

$[1\bar{1}0]$  at  $z = 0$ , or those at  $z = 1/2$  to point along  $[110]$ . Two neighboring apexes create  $M$ -O-O- $M$  linkages that are important for the formation of the 1D antiferromagnetic chains [14]; these linkages are evident upon inspection of Fig. 1.

Band structure calculations for  $\text{CuSb}_2\text{O}_6$  reveal an unusual quasi-1D magnetic ground state driven by orbital ordering, which is attributed to the presence of competing interactions between in- and out-of-plaquette orbitals and strong electron correlations [14]. The calculations suggest that the dominant magnetic exchange is along the  $[110]$  crystallographic direction at  $z = 0$  and the  $[1\bar{1}0]$  direction at  $z = 1/2$ . It is therefore directed along the apexes of the  $\text{Cu-O}_6$  octahedra (i.e., via the out-of-plaquette oxygen) producing  $\text{Cu-O-O-Cu}$  linkages within the crystal structure. The directional aspect of the magnetic exchange suggests a *two-sublattice model* for the antiferromagnetic structure. One sublattice, at  $z = 0$ , has antiparallel magnetic moments along  $[110]$  with the moments lying purely in the  $a$ - $b$  plane (i.e., no canting along  $[001]$ ); the second magnetic sublattice, at  $z = 1/2$ , has its moments also lying purely in the  $a$ - $b$  plane, but rotated  $90^\circ$  with regard to the first layer. Upon viewing Fig. 1, it becomes clear how this magnetic structure can occur via the  $M$ -O-O- $M$  linkages, since the chains at  $z = 0$  and  $z = 1/2$  are perpendicular to one another. Band structure calculations [14] suggest  $J/J_\perp \sim 120$  for  $\text{CuSb}_2\text{O}_6$  [29].

There is disagreement regarding the magnetically ordered state in  $\text{CuSb}_2\text{O}_6$  determined from experiment. Nakua and Greedan [11] proposed two possible magnetic structures, based on powder neutron diffraction data. One of these,

the *orthogonal model*, has Cu magnetic moments ordered antiparallel along  $[110]$  at  $z = 0$  and  $[1\bar{1}0]$  at  $z = 1/2$ ; it is identical to the two-sublattice model described above. Later, single-crystal neutron diffraction by Kato *et al.* [7] determined that the magnetic structure involved parallel alignment (i.e., ferromagnetic) of the magnetic moments along  $[010]$ , with adjacent moments aligned antiparallel [i.e., forming an antiferromagnetic structure with magnetic wave vector  $(\pi/a, 0, \pi/c)$ ]. Subsequent single-crystal measurements by Gibson *et al.* [12] suggested ordering similar to the two-sublattice model, albeit with a slight tilting of the moments. The work by Kato *et al.* is the most detailed investigation/analysis, and their magnetic structure model agrees best with the anisotropy [9] of the magnetic susceptibility  $\chi$  (see discussion of  $\chi$  below). More recent neutron diffraction experiments [28] also agree with Kato *et al.* This model, however, disagrees with the magnetic structure suggested by the magnetic exchange constants obtained from band structure calculations [14].

In the case of  $\text{NiTa}_2\text{O}_6$ , density functional theory (DFT) calculations [15] reveal  $J/J_\perp \sim 65$  and that the dominant antiferromagnetic exchange path is along  $[110]$  at  $z = 0$  and  $[1\bar{1}0]$  at  $z = 1/2$ , which would result in the same two-sublattice model (or orthogonal model) for the antiferromagnetic structure as described above [29]. In the same work, however, results from powder neutron diffraction (PND) revealed the antiferromagnetic structure previously reported by Ehrenberg *et al.* [26], also based on PND data, where the Ni magnetic moments are ordered antiparallel along  $[110]$  at  $z = 0$  and  $z = 1/2$ . This discrepancy was not addressed [15].

However, the DFT calculations and the absence of Ni-O-O-Ni bonds along [110] at  $z = 1/2$ , as noted above, provide support for the two-sublattice model. Neutron diffraction on single crystals will likely be required to identify the antiferromagnetic structure with better certainty, given the presence of disorder below  $T_N$  in the PND data [26].

The magnetically ordered state of  $\text{CoSb}_2\text{O}_6$  also displays superexchange pathways along [110] (i.e., along Co-O-O-Co linkages), with a magnetic structure [8] that is described as similar to that of  $\text{FeTa}_2\text{O}_6$ . However, two magnetic structures were proposed [30] for  $\text{FeTa}_2\text{O}_6$  and Mössbauer effect data suggest canting of the magnetic moments by  $20^\circ$  in the [001] direction [1]. Of the proposed structures, one is identical to the two-sublattice model described above. Neither of these structures included any canting in the [001] direction. At present, no estimates of  $J/J_\perp$  exist for  $\text{CoSb}_2\text{O}_6$ .

The brief review provided above reveals that more experiments are required to identify the antiferromagnetic structures of  $\text{CuSb}_2\text{O}_6$ ,  $\text{NiTa}_2\text{O}_6$ , and  $\text{CoSb}_2\text{O}_6$ . In the present work, analysis of the magnetic susceptibility data of our single-crystalline samples helps to infer the most probable antiferromagnetic structures for the three compounds from among the proposed structures. Heat capacity measurements for differing orientations of magnetic field  $H$  with regard to the quasi-1D magnetic chains lends support for the inferred structures. The two-sublattice model is found to be valid for  $\text{NiTa}_2\text{O}_6$  and  $\text{CoSb}_2\text{O}_6$ , but not for  $\text{CuSb}_2\text{O}_6$ .

Determination of the antiferromagnetic structures is an important step toward understanding the physical properties of these compounds. The weak coupling between the sublattices in the quasi-1D magnetic solids  $\text{NiTa}_2\text{O}_6$  and  $\text{CoSb}_2\text{O}_6$  leads to the presence of two antiferromagnetic transitions when the magnetic field  $H$  is parallel to the quasi-1D chains of one lattice and perpendicular to the those of the second. The typical magnetic field required to disrupt the magnetic ordering along the chain is about 2 T, which corresponds to an energy on the order of 0.2 meV. The effect is associated with competition among Néel, dimer, and spin-liquid states that are all present at  $T_N$ .

The shift of the integrated intensity of the magnetic-ordering peak in the heat capacity at constant pressure  $C_P$  with temperature through the application of magnetic field implies a change in magnetic entropy, which in turn indicates the presence of a magnetocaloric effect (MCE). The MCE is investigated through analysis of  $C_P$  and magnetization data. The anisotropy of the observed MCE suggests that rotating the sample in constant magnetic field would cause it to cool or warm, such as revealed [31,32] for  $\text{NdCo}_5$ ,  $\text{ErGa}_2$ , and  $\text{HoGa}_2$ . However, in the compounds studied in the present work, the MCE is associated with the orientation of each sublattice with regard to  $H$ , the presence of magnetic frustration within each sublattice, and the poor magnetic coupling between adjacent sublattices. The absence of a MCE in  $\text{CuSb}_2\text{O}_6$  is attributed to its different antiferromagnetic structure, more robust magnetic exchange, and its propensity to exhibit a spin-flop transition [9]. The MCE reported herein differs from that observed [33] and theoretically studied [34–37] for low-dimensional quantum-spin systems, where saturation to a fully polarized magnetic system is responsible.

The organization of this report is as follows. Section II highlights experimental and sample preparation methods. Section III discusses magnetic susceptibility data with the goal of determining which of the proposed antiferromagnetic structures for each compound is most probable. Section IV presents and discusses the magnetic portion of the heat capacity data on  $\text{NiTa}_2\text{O}_6$  and  $\text{CoSb}_2\text{O}_6$  in order to highlight the large amount of short-range magnetic order present near  $T_N$ . This issue has been addressed for  $\text{CuSb}_2\text{O}_6$  in prior work [9]. These sections form the necessary prelude to understanding the influence of magnetic field on the heat capacity of  $\text{CuSb}_2\text{O}_6$ ,  $\text{NiTa}_2\text{O}_6$  and  $\text{CoSb}_2\text{O}_6$ , which forms the topic of Sec. V, where data and interpretation thereof are presented. Finally, an important by-product of this work is the existence of a magnetocaloric effect that is discussed in Sec. VI, which is followed by a brief summary and outlook in Sec. VII.

## II. EXPERIMENTAL DETAILS

Single crystals of  $\text{CuSb}_2\text{O}_6$  and  $\text{CoSb}_2\text{O}_6$  were grown using chemical vapor transport as described previously [9,13,38]. Polycrystalline  $\text{NiTa}_2\text{O}_6$  was synthesized by mixing stoichiometric quantities of NiO and  $\text{Ta}_2\text{O}_5$  in an agate mortar followed by heating to  $1050^\circ\text{C}$  for 23 hours in air. The sample was reground, pelletized and reacted for 48 hours in air at  $1100^\circ\text{C}$ . This step was repeated twice with successively higher reaction temperatures of  $1150^\circ\text{C}$  and  $1200^\circ\text{C}$ . The sample was then reground and hydrostatically pressed at 40 MPa into 3 mm diameter rods up to 60 mm in length followed by sintering at  $1100^\circ\text{C}$  for 10 hours and  $1200^\circ\text{C}$  for 20 hours. Single crystals of  $\text{NiTa}_2\text{O}_6$  were then grown from the polycrystalline rods using the floating-zone method utilizing a two-lamp image furnace with 1500 W halogen lamps operating at 570 W in a flowing oxygen atmosphere at 0.21 MPa. The growth rate was 5 mm/h and rotation rates of 30 rpm for both the feed and seed rod were used. A single crystal of  $\text{ZnSb}_2\text{O}_6$ , prepared as described previously [9], was used as a nonmagnetic analog for data analysis purposes. All crystals were oriented using Laue x-ray diffraction. A polycrystalline sample of  $\text{MgTa}_2\text{O}_6$  was prepared by mixing stoichiometric quantities of MgO and  $\text{Ta}_2\text{O}_5$  followed by heating to  $1000^\circ\text{C}$  for 10 hours in air. The sample was reground, pelletized, and reacted for 96 hours in air at  $1000^\circ\text{C}$ . Subsequently, the sample was reground, pelletized, and reacted for 480 hours in air at  $1050^\circ\text{C}$ . Phase purity of the samples was checked with x-ray diffraction. All measurements utilized a Quantum Design physical properties measurement system; this device uses vibrating sample magnetometry to measure magnetic susceptibility and the heat-pulse technique to measure heat capacity.

## III. MAGNETIC SUSCEPTIBILITY

The magnetic susceptibility  $\chi$  of  $\text{CuSb}_2\text{O}_6$ ,  $\text{NiTa}_2\text{O}_6$ , and  $\text{CoSb}_2\text{O}_6$  at 0.2 T is shown in Fig. 2. The data were corrected for the core diamagnetism, and plotted as  $1/\chi$  versus  $T$  (not shown) in order to conduct Curie-Weiss fits. Those fits were carried out over the temperature range above 100 K. They reveal magnetic moments consistent with total spin on the transition-metal site  $S = 1/2$ , 1, and  $3/2$  for  $\text{CuSb}_2\text{O}_6$ ,

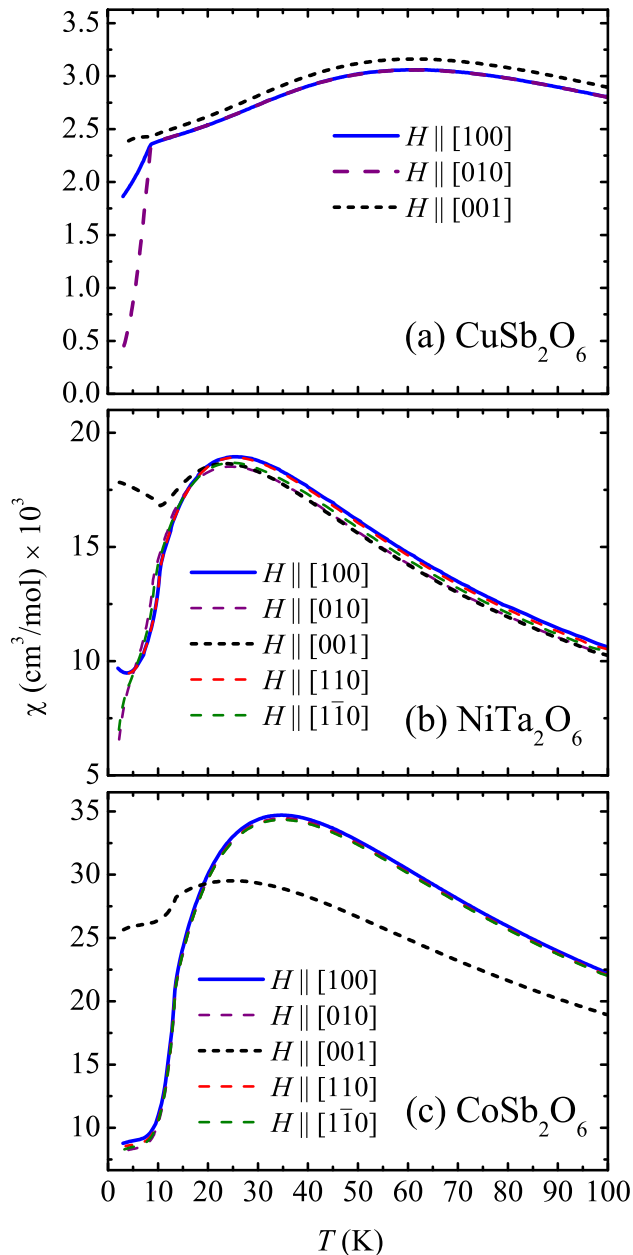


FIG. 2. (Color online) Magnetic susceptibility  $\chi$  versus temperature  $T$  for (a)  $\text{CuSb}_2\text{O}_6$ , (b)  $\text{NiTa}_2\text{O}_6$ , and (c)  $\text{CoSb}_2\text{O}_6$  in a magnetic field  $H$  of 0.2 T. The directions of  $H$  with regard to the respective crystallographic directions are indicated in the legends.

$\text{NiTa}_2\text{O}_6$ , and  $\text{CoSb}_2\text{O}_6$ , respectively [13]. Antiferromagnetic order occurs at  $T_N = 8.5$  K, 10.5 K, and 13.5 K for  $\text{CuSb}_2\text{O}_6$ ,  $\text{NiTa}_2\text{O}_6$ , and  $\text{CoSb}_2\text{O}_6$ , respectively, as noted above.  $\chi$  was measured along multiple crystallographic directions for each specimen to investigate its anisotropy.

$\text{CuSb}_2\text{O}_6$  exhibits significant anisotropy below  $T_N$  for  $H$  applied along each of its principal crystallographic directions. Normally when  $H$  is applied perpendicular to the axis along which the moments lie in their antiferromagnetically ordered state,  $\chi$  approaches a constant [39]. If  $H$  is applied parallel to the axis along which the moments lie,  $\chi \rightarrow 0$  as  $T \rightarrow 0$  [39]. Thus, through inspection of the temperature dependence of  $\chi$

below  $T_N$  as  $T \rightarrow 0$ , information regarding the alignment of the moments in their ordered state with regard to  $H$  can be inferred. The data in Fig. 2(a) reveal that  $\chi$  fails to clearly tend toward zero for any of the applied field directions. Obviously the moments seem to be ordered perpendicular to [001] (i.e., perpendicular to the  $c$  direction), but  $\chi$ 's behavior as  $T \rightarrow 0$  implies that the moments are *not* aligned parallel to either [100] or [010] (i.e., parallel to the  $a$  or  $b$  axes, respectively). However, the decrease of  $\chi$  below  $T_N$  for  $H$  applied along [010] is significantly stronger than for  $H$  applied along [100]. Therefore, it seems reasonable to deduce that the alignment of the moments in  $\text{CuSb}_2\text{O}_6$  is nearly parallel to [010], which agrees best with two of the neutron diffraction data analyses [7,28]. The data in Fig. 2 may suggest a slight deviation of the moment alignment with regard to [010], which could be associated with the monoclinic distortion.

Inspection of the  $\chi$  data for  $\text{NiTa}_2\text{O}_6$  [see Fig. 2(b)] as  $T \rightarrow 0$  below  $T_N$  reveal a more complex situation. Clearly the saturation of  $\chi$  for  $H \parallel [001]$  indicates that the magnetic moments appear to be aligned perpendicular to [001]. The data for  $H$  applied along [100] and [110] suggest that the moments are not aligned along either of these directions. For  $H$  applied along [010] and  $[1\bar{1}0]$ ,  $\chi$  below  $T_N$  decreases further toward zero, suggesting that the moment alignment along those directions is better, but clearly these are also *not* the directions along which *all* of the moments are aligned. Similar behavior occurs for  $\text{CoSb}_2\text{O}_6$ , as shown in Fig. 2(c). No canting of the magnetic moments along [001], as proposed [1], seems evident from the  $\chi$  data for  $H \parallel [001]$ . For magnetic field  $H$  applied along [100], [010], [110], and  $[1\bar{1}0]$ , all  $\chi$  data behave similarly. As with  $\text{NiTa}_2\text{O}_6$ , the Co magnetic moments of  $\text{CoSb}_2\text{O}_6$  appear to be better aligned with directions lying in the  $a$ - $b$ -plane than with  $c$ , but clearly there is not a single direction among those measured along which *all* of the moments are aligned.

The two-sublattice model for antiferromagnetic ordering discussed above seems an appropriate model to describe the behavior of  $\chi$  below  $T_N$  for  $\text{NiTa}_2\text{O}_6$  and  $\text{CoSb}_2\text{O}_6$ . In this model,  $H$  is never directed along the axis for which *all* of the antiparallel magnetic moments are aligned for any of the measured field directions shown in Figs. 2(b) and 2(c). The case for this two-sublattice model in  $\text{CoSb}_2\text{O}_6$  is slightly more convincing than for  $\text{NiTa}_2\text{O}_6$ , since  $\chi$  for all four measured directions within the  $a$ - $b$  plane are identical. The data in Fig. 2(b) may indicate disorder of the moments, or slight canting from the [110] and  $[1\bar{1}0]$  directions in the respective sublattices in  $\text{NiTa}_2\text{O}_6$ . Although the  $\chi$  data do not provide absolute proof of the two-sublattice model, further support is provided from the  $C_P$  data presented in Sec. V.

#### IV. MAGNETIC ENTROPY

$C_P$  data of  $\text{CuSb}_2\text{O}_6$  were reported in prior work [9] and are briefly summarized here. The magnetic contribution to  $C_P$ , referred to as the magnetic heat capacity  $\delta C_P$ , was obtained by subtracting  $C_P$  data for the nonmagnetic analog compound  $\text{ZnSb}_2\text{O}_6$  from the  $\text{CuSb}_2\text{O}_6$  data. The results are surprising in that 58% of the expected magnetic entropy change of  $R \ln 2$  occurred over the region between 115 K and  $T_N$ , with the majority of that entropy change occurring between 50 K and

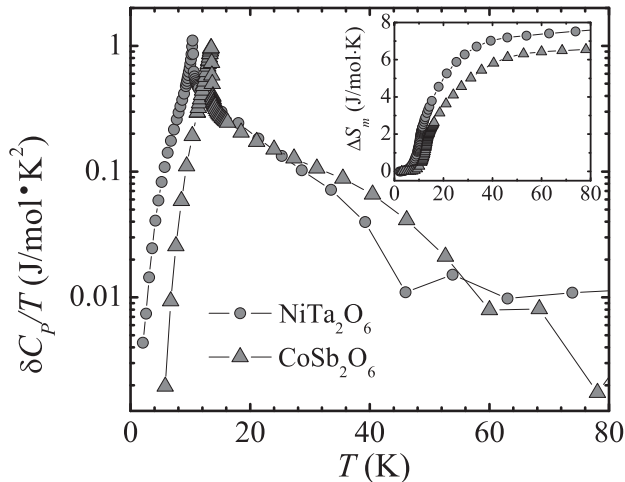


FIG. 3. Magnetic contribution to the heat capacity of  $\text{NiTa}_2\text{O}_6$  and  $\text{CoSb}_2\text{O}_6$ . Data are shown on a log scale to emphasize the shoulder above  $T_N$  due to short-range order. Inset displays the magnetic entropy change  $\Delta S_m$ , which was determined from the area under the curves in the main panel.

$T_N$ . An additional 9% change in magnetic entropy occurred on cooling below  $T_N$  to 0.4 K, for a total magnetic entropy change of 67% of  $R \ln 2$ . This clearly illustrates the presence of a substantial amount of short-range magnetic order above  $T_N$  as well as a significant number of unordered spins at the lowest temperature. Furthermore, below  $T_N$  an energy gap of 1.15 meV was observed. The gap was attributed to coupling between the 1D Jordan-Wigner-transformed fermions and the 3D phonons. The magnetic ordering at  $T_N$  was viewed as an alignment of the 1D chains, rather than the formation of a truly 3D magnetically ordered state.

Figure 3, which shows  $\delta C_P/T$  versus  $T$  for  $\text{NiTa}_2\text{O}_6$  and  $\text{CoSb}_2\text{O}_6$ , reveals a great deal of similarity to the data of  $\text{CuSb}_2\text{O}_6$ . The nonmagnetic analog compounds used for the analysis were  $\text{MgTa}_2\text{O}_6$  and  $\text{ZnSb}_2\text{O}_6$ , respectively. In the region between 80 K and  $T_N$ ,  $\text{NiTa}_2\text{O}_6$  experiences a loss in magnetic entropy that is 62% of  $R \ln(2S + 1)$ , while measurements from  $T_N$  to the lowest measured temperature reveal an additional entropy loss of only 20%. In the case of  $\text{CoSb}_2\text{O}_6$ , between 80 K and  $T_N$  an entropy loss of 42% is observed and below  $T_N$  the additional entropy loss is 15%. Thus, the data reveal the short-range order above  $T_N$  as a very dominant physical property of all three of these systems, with the long-range order below  $T_N$  as a relatively minor further reduction of the entropy.

In lieu of these observations, it seems reasonable to assert that strong magnetic frustration is present in the vicinity of  $T_N$  for all of these compounds. The magnetic system must involve Néel ordered regions (i.e., long-range antiferromagnetic ordering), short-range ordered regions, and unordered regions. The unique antiferromagnetic structure of  $\text{NiTa}_2\text{O}_6$  and  $\text{CoSb}_2\text{O}_6$  is expected to play a role in generating magnetic frustration, since the  $90^\circ$  orientation of alternating chains along  $c$  would most likely weaken the magnetic coupling along this direction, leading to a less robust ordered state below  $T_N$ . The weak magnetic exchange [15] within the  $a$ - $b$  plane, but in directions other than the chain direction, must also play a role. The nature of the

short-range order is probably in the form of dimers, or larger collections of magnetic moments, separated by disordered spins, which can be thought of as a spin liquid. The spin-liquid state is essentially a collection of frustrated spins [23–25]. At  $T_N$  and below, the relatively modest change in entropy suggests that the Néel, dimer, and spin-liquid states coexist.

## V. INFLUENCE OF MAGNETIC FIELD ON ANTIFERROMAGNETIC ORDERING

Measurements of heat capacity at constant pressure  $C_P$  were used to investigate the effect of  $H$  on the antiferromagnetic ordering. Furthermore,  $C_P$  was measured for  $H$  applied along a number of crystallographic directions for each specimen to investigate the anisotropic effect of  $H$  on magnetic ordering. Figure 4(a) reveals the influence of  $H$  on  $C_P$  in  $\text{CuSb}_2\text{O}_6$  for  $H$  applied along the [100], [010], and [001] directions. For  $H = 0$ , a peak associated with long-range antiferromagnetic order occurs in  $C_P$  at  $T_N = 8.5$  K. The peak is not affected appreciably by magnetic field ( $H \leq 8$  T) for any of the measured directions.

Data for  $C_P$  of  $\text{NiTa}_2\text{O}_6$  are shown in Fig. 4(b). When  $H \parallel [001]$ , there is a single peak in  $C_P$  at  $T_N$  upon which application of field has little or no influence [see inset of Fig. 4(b)]. For  $H \parallel [110]$  very different behavior is observed. For  $H > 2$  T, the single peak in  $C_P$  splits into two, with one peak remaining at the position of the  $H = 0$  peak, and the second peak moving to lower  $T$  with increase of  $H$ . At the same time, the original peak reduces in integrated intensity with the lost intensity emerging in the newly formed peak. The effect is identical for  $H \parallel [1\bar{1}0]$  (data for this direction are not shown, for clarity). When  $C_P$  is measured at 8 T for  $H \parallel [100]$  [see the gray dashed curve in Fig. 4(b)] a single, asymmetric peak is evident. It shifts to lower temperature with increasing field, but the shift is approximately midway between the two peaks in the  $H \parallel [110]$  data. The peak's asymmetry may be associated with misalignment of the sample with respect to  $H$ . Law *et al.* [15] measured heat capacity in magnetic field on a polycrystalline sample of  $\text{NiTa}_2\text{O}_6$  and observed the peak in  $C_P$  at  $T_N$  to smear out. In light of the observations herein, the behavior they observed is expected.

Figure 4(c) shows  $C_P$  data for  $\text{CoSb}_2\text{O}_6$ , which reveals behavior that is very similar to that of  $\text{NiTa}_2\text{O}_6$ . When  $H \parallel [001]$ , there is a single peak in  $C_P$  at  $T_N$  upon which application of field has little or no influence [see inset of Fig. 4(c)]. For  $H \geq 2$  T, the single peak in  $C_P$  splits into two only for  $H \parallel [110]$  or  $[1\bar{1}0]$  (data for the  $[1\bar{1}0]$  direction are not shown). The newly formed peak in  $\text{CoSb}_2\text{O}_6$  is much sharper than the corresponding peak in  $\text{NiTa}_2\text{O}_6$ . This may be associated with better order among the moments in the two-sublattice model discussed in Sec. III. For  $H \parallel [100]$  or  $[010]$  (latter not shown), only a single asymmetric peak is evident [see the gray dashed curve in Fig. 4(c)]; it shifts to lower temperature with increasing field, with the shift midway between the two peaks in the  $H \parallel [110]$  data of Fig. 4(c).

Focusing for a moment on the data for  $H \parallel c$ , since the magnetic moments lie in the  $a$ - $b$  plane, and the magnetic exchange within the  $a$ - $b$  plane is dominant [14,15], there is minimal affect on the position or shape of the peak in  $C_P$  for any of the specimens when  $H \parallel [001]$ . The differing

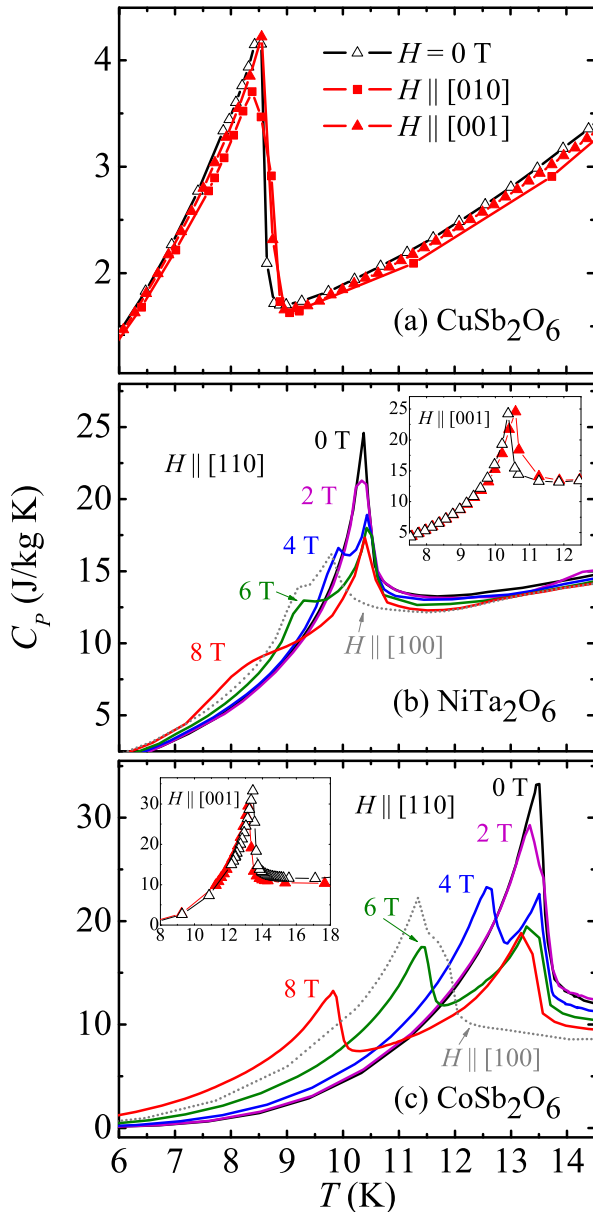


FIG. 4. (Color online) Heat capacity  $C_P$  of (a)  $\text{CuSb}_2\text{O}_6$ , (b)  $\text{NiTa}_2\text{O}_6$ , and (c)  $\text{CoSb}_2\text{O}_6$ . (a) Data are shown for  $\text{CuSb}_2\text{O}_6$  at  $H = 0$  (open data points) and 8 T (filled red data points) for  $H \parallel [010]$  and  $[001]$ ; no field-induced shift in temperature of the peak in  $C_P$  is observed. For (b)  $\text{NiTa}_2\text{O}_6$  and (c)  $\text{CoSb}_2\text{O}_6$ , data for  $H \parallel [001]$  at  $H = 0$  (open data points) and  $H = 8$  T (filled red data points) are shown in the insets; no appreciable shift in the peak in  $C_P$  occurs. For  $H \parallel [110]$ , (b) and (c) show that two peaks emerge in the  $C_P$  data as magnetic field is increased in magnitude. This is most clearly evident in panel (c) for  $\text{CoSb}_2\text{O}_6$ . The gray dotted lines in (b) and (c) show data for  $H \parallel [100]$  at 8 T.

behavior of  $\text{CuSb}_2\text{O}_6$  for  $H$  applied within the  $a$ - $b$  plane can be associated with a few distinct differences it has when compared to the other two compounds. As discussed above, it appears that the antiferromagnetic structure of  $\text{CuSb}_2\text{O}_6$  may not be the two-sublattice structure. In addition,  $\text{CuSb}_2\text{O}_6$  exhibits [9] a spin-flop transition for  $H \parallel [100]$  or  $[010]$  at  $H = 1.3$  T. This

transition allows  $\text{CuSb}_2\text{O}_6$  to lower its energy in the presence of  $H$  without a noticeable reduction of  $T_N$  (i.e., without a shift in the magnetic-ordering peak in  $C_P$ ). Finally, the magnetic exchange constants [14,15]  $J_{[110]}$ ,  $J_{[100]}$ , and  $J_{[\frac{1}{2}\frac{1}{2}\frac{1}{2}]}$  are four to twelve times larger in magnitude for  $\text{CuSb}_2\text{O}_6$  versus those for  $\text{NiTa}_2\text{O}_6$ . Thus, the magnetic coupling within the plane, and with the neighboring plane, is more robust in  $\text{CuSb}_2\text{O}_6$ , which will make the antiferromagnetic ordering temperature in  $\text{CuSb}_2\text{O}_6$  more resistant to  $H$ . At the same time, the magnetic exchange constant between the next-nearest planes in  $\text{NiTa}_2\text{O}_6$  is slightly stronger. Note that these comparisons of magnetic exchange constants assume that  $\text{CuSb}_2\text{O}_6$  possesses two-sublattice antiferromagnetic ordering [14], which requires further investigation. However, the comparisons provide a sense of why magnetic field might have a more pronounced influence on the antiferromagnetic state of  $\text{NiTa}_2\text{O}_6$ .

An explanation for the formation of two peaks when  $H \parallel [110]$  or  $[1\bar{1}0]$  is now proposed. In the two-sublattice model for antiferromagnetic ordering in  $\text{NiTa}_2\text{O}_6$  and  $\text{CoSb}_2\text{O}_6$ , one lattice, at  $z = 0$ , has its magnetic moments oriented parallel to  $[110]$  with neighboring moments rotated  $180^\circ$  with regard to one another. The adjacent magnetic layer, at  $z = 1/2$ , has its moments lying in the  $a$ - $b$  plane, but rotated  $90^\circ$  with regard to the  $z = 0$  layer. The magnetic moments are directed naturally along the  $M$ - $O$ - $O$ - $M$  linkages shown in Fig. 1. When  $H \parallel [110]$  or  $[1\bar{1}0]$ ,  $H$  is parallel to the moment axis of one sublattice, but oriented  $90^\circ$  with regard to the second. The magnetic heat capacity data in Sec. IV reveal the presence of a substantial amount of short-range magnetic order immediately above  $T_N$ , and the fact that little additional entropy loss occurs on further cooling below  $T_N$ . Thus, the magnetic ordering in  $\text{NiTa}_2\text{O}_6$  and  $\text{CoSb}_2\text{O}_6$  at  $T_N$ , as well as the ordered state below, can be viewed as a collection of short-range ordered regions that have aligned to form the two-sublattice antiferromagnetic state. However, within this *ordered* state, 15% or more of the magnetic moments remain unordered, even to the lowest temperatures measured herein. These unordered magnetic moments comprise the spin-liquid state described in Sec. IV.

Application of magnetic field parallel to a chain would help to order some of the moments of the spin-liquid state, thereby stabilizing the Néel state. In contrast, application of  $H$  perpendicular to a chain would enhance the magnetic frustration, thereby destabilizing the Néel state. As a result, the magnetic entropy change for the magnetic moments at  $T_N$  on half of the chains will move downward in temperature to a region where less thermal energy is present. When  $H \parallel [100]$  or  $[010]$ ,  $H$  is at an angle of  $45^\circ$  with respect to both sublattices. As a result,  $T_N$  is suppressed uniformly for both, and only one peak appears in  $C_P$ . Some asymmetry in this peak is likely associated with slight misalignment of the sample with respect to  $H$ . Note that no shift in the  $C_P$  peak occurs if  $H \parallel [001]$ . This indicates that the moments are constrained to lie in the  $a$ - $b$  plane, and little magnetic frustration occurs in the out-of-plane direction.

Relatively weak interlayer coupling [15] along  $[\frac{1}{2}\frac{1}{2}\frac{1}{2}]$  in  $\text{NiTa}_2\text{O}_6$  (when compared [14] to  $\text{CuSb}_2\text{O}_6$ ) isolates the sublattices from one another, allowing the magnetic moments of each sublattice to act in a relatively independent manner from

those of neighboring sublattices. The weak coupling between the sublattices along the  $[\frac{1}{2}\frac{1}{2}\frac{1}{2}]$  direction [15] in  $\text{NiTa}_2\text{O}_6$  of  $\sim 0.5$  K is comparable to  $\mu H/k_B \sim 1.3$  K at 1 T (assuming  $\mu = 2\mu_B$  for the Ni magnetic moment, where  $\mu_B$  is the Bohr magneton and  $k_B$  is the Boltzmann constant), which allows fields in the range used here to disrupt the magnetic ordering along [001]. This relationship between the two energy scales is less favorable for  $\text{CuSb}_2\text{O}_6$ , where [14]  $J_{[\frac{1}{2}\frac{1}{2}\frac{1}{2}]} \sim 3.3$  K and  $\mu H/k_B \sim 0.7$  K at 1 T; note that the 8 T field used in this work reaches the necessary energy range, so the absence of an effect of 8 T on the peak in  $C_P$  provides additional evidence against the two-sublattice model for  $\text{CuSb}_2\text{O}_6$ . This discussion reveals that the  $C_P$  data presented herein provide strong support for the two-sublattice model of antiferromagnetic order in  $\text{NiTa}_2\text{O}_6$  and  $\text{CoSb}_2\text{O}_6$  presented in Sec. III. Calculations of band structure and magnetic exchange constants for  $\text{CoSb}_2\text{O}_6$  are unavailable at present; they would be valuable in evaluating the model described above, but are beyond the scope of this report.

## VI. MAGNETOCALORIC EFFECT

The observation that the integrated intensity of the peak in  $C_P$  associated with antiferromagnetic ordering shifts to lower temperature with application of  $H$  implies that there exists a change in magnetic entropy  $\Delta S_m$ , and a magnetocaloric effect (MCE). The MCE can be evaluated by analyzing the  $C_P$  data. The entropy change over a specific temperature range at constant  $H$  is calculated from  $C_P$  using

$$\Delta S_T(H) = \int_{T_1}^{T_2} \left( \frac{C_P(T, H)}{T} \right) dT. \quad (1)$$

The results from Eq. (1) are then used to determine the change in magnetic entropy  $\Delta S_m(\Delta H) = \Delta S_T(H_2) - \Delta S_T(H_1)$  associated with the change in magnetic field  $\Delta H = H_2 - H_1$ . Beginning the integration of Eq. (1) at the lowest measurement temperature  $T_1$ , and terminating at any finite temperature  $T > T_1$ , allows determination of  $\Delta S_m(T, \Delta H)$ .

The magnetic entropy change can also be calculated using  $\chi$  data, after converting it into units of magnetization  $M$ . This can be appreciated through the Maxwell relation

$$\left( \frac{\partial M}{\partial T} \right)_H = \left( \frac{\partial S_m}{\partial H} \right)_T. \quad (2)$$

The change in  $S_m$  associated with a change in  $H$  is determined by integrating Eq. (2) to obtain

$$\Delta S_m(T, \Delta H) = \int_{H_1}^{H_2} \left( \frac{\partial M}{\partial T} \right)_H dH. \quad (3)$$

In practice, Eq. (3) is used to determine  $\Delta S_m(T, \Delta H)$  at any temperature  $T$  for a specific field change  $\Delta H = H_2 - H_1$ . Note that  $H_1$  is small but nonzero, since a finite  $H$  is required to measure  $M$ .

$M$  was measured in fields of 0.2, 2, 4, 6, and 8 T, and only upon cooling at rates of 0.8 K/min to ensure consistency. A plot of  $(\partial M/\partial T)_H$  for all samples is shown in Fig. 5. Data for  $\text{CuSb}_2\text{O}_6$  at 0.2 T and the maximum field of 8 T for  $H \parallel [100]$ , [010], and [001] are shown in Fig. 5(a).  $(\partial M/\partial T)_H$  is strongly

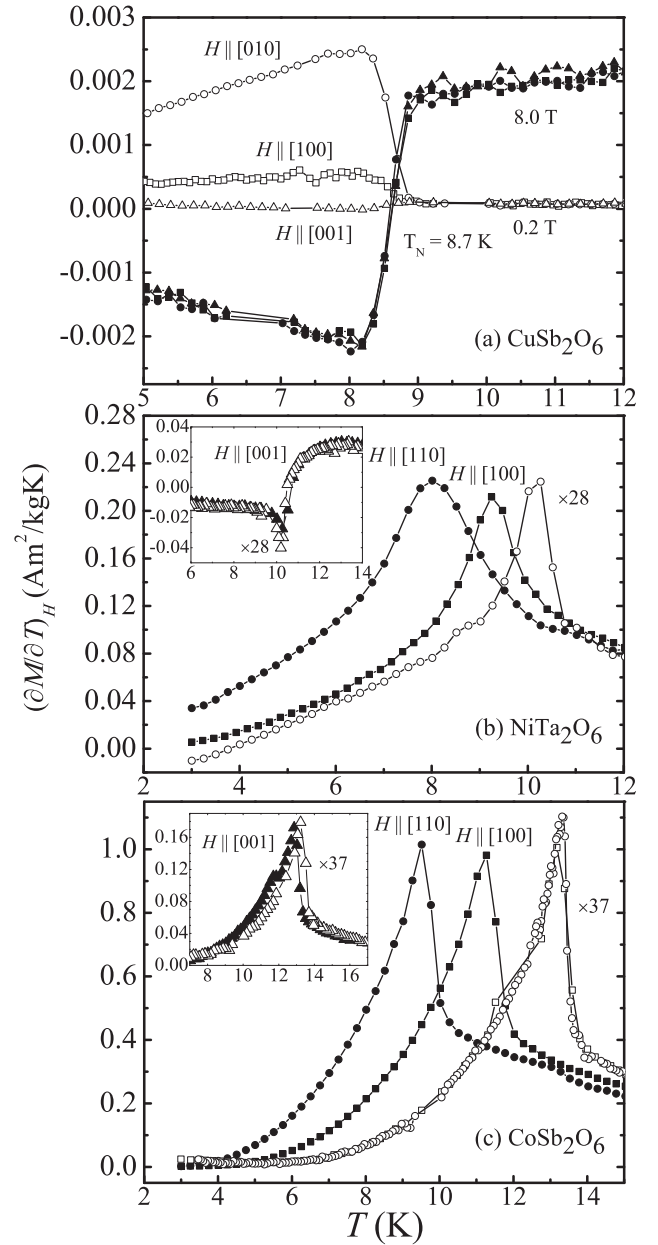


FIG. 5. Temperature derivative of the magnetization,  $(\partial M/\partial T)_H$ , for (a)  $\text{CuSb}_2\text{O}_6$ , (b)  $\text{NiTa}_2\text{O}_6$ , and (c)  $\text{CoSb}_2\text{O}_6$ . Data for  $H \parallel [100]$ , [001], and [110] axes are represented by squares, triangles, and circles, respectively. For  $\text{NiTa}_2\text{O}_6$  and  $\text{CoSb}_2\text{O}_6$ , the curves for  $H \parallel [100]$  and [010] are identical in all fields. Therefore, data for  $H \parallel [010]$  are not shown. Likewise, curves for  $H \parallel [110]$  and  $[1\bar{1}0]$  are identical and the  $H \parallel [1\bar{1}0]$  curves are not shown. Open data points represent measurements at  $H = 0.2$  T; these data have been multiplied by 28 and 37, as indicated, to improve visibility. Filled data points represent measurements at  $H = 8$  T.

influenced by the increase in  $H$ , but the temperature where the steep change in  $(\partial M/\partial T)_H$  occurs is negligibly affected. This is consistent with the measurements of  $C_P$  discussed above, which indicate little influence of  $H$  on the position of the peak at  $T_N$  associated with magnetic ordering. The maximum magnitude of  $(\partial M/\partial T)_H$  for  $\text{CuSb}_2\text{O}_6$  is 120 to 500

times smaller than that observed for NiTa<sub>2</sub>O<sub>6</sub> and CoSb<sub>2</sub>O<sub>6</sub> [see Figs. 5(b) and 5(c)]. Upon consideration of Eq. (3), the small magnitude of  $(\partial M/\partial T)_H$  signifies an extremely small magnetocaloric effect for CuSb<sub>2</sub>O<sub>6</sub>.

The situation is very different for NiTa<sub>2</sub>O<sub>6</sub> and CoSb<sub>2</sub>O<sub>6</sub>. A clear shift of  $(\partial M/\partial T)_H$  to lower temperature occurs for NiTa<sub>2</sub>O<sub>6</sub> and CoSb<sub>2</sub>O<sub>6</sub> when magnetic field lies in the *a-b* plane, as shown in Figs. 5(b) and 5(c). On the other hand, when  $H \parallel [001]$  the shift in temperature of  $(\partial M/\partial T)_H$  is negligible [see insets of Figs. 5(b) and 5(c)], which, upon consideration of Eqs. (1) and (3), is consistent with the  $C_P$  data discussed above. Any shift of  $(\partial M/\partial T)_H$  for  $H \parallel [001]$  can likely be attributed to misalignment of the single-crystal axes with regard to  $H$ . The shift of the maximum of  $(\partial M/\partial T)_H$  is greatest ( $\Delta T = 2.1$  K for NiTa<sub>2</sub>O<sub>6</sub> and 3.8 K for CoSb<sub>2</sub>O<sub>6</sub>) when the field is along either [110] or  $[1\bar{1}0]$ . This shift is about twice that for  $H \parallel [100]$  or  $[010]$  ( $\Delta T \approx 0.9$  K and  $\Delta T \approx 2$  K for NiTa<sub>2</sub>O<sub>6</sub> and CoSb<sub>2</sub>O<sub>6</sub>, respectively). This behavior is expected, based on the  $C_P$  data and discussion of the two-sublattice model in Sec. V.

It is interesting to note that a small bump can be seen at  $\sim 11.0$  K for NiTa<sub>2</sub>O<sub>6</sub> and  $\sim 13.2$  K for CoSb<sub>2</sub>O<sub>6</sub> in the  $(\partial M/\partial T)_H$  measurements with 6 T (not shown) and 8 T along [110] and  $[1\bar{1}0]$ . These bumps do not shift in temperature as the field is increased from 6 to 8 T. Such a bump is not immediately observed at lower fields because the main peak overlaps this region. These bumps are associated with the original  $C_P$  peak at  $T_N$ , which does not shift in  $T$ , but loses intensity to the formation of the secondary peak [see Figs. 4(b) and 4(c)]. The bump in  $(\partial M/\partial T)_H$  is not observed for  $H \parallel [100]$ ,  $[010]$ , or  $[001]$ , in agreement with the absence of two peaks in  $C_P$  when  $H$  is parallel to the same axes. The fact that the peaks in  $C_P$  are more prominent than the bumps in  $(\partial M/\partial T)_H$  can be appreciated upon careful consideration of Eqs. (1) and (3), and their use in determining  $\Delta S_M$ . Furthermore, the peak in  $(\partial M/\partial T)_H$  is associated with magnetic moments oriented parallel to  $H$ ; therefore, their response upon cooling below their ordering temperature is more pronounced [39] than for those perpendicular to  $H$ .

The quantity  $|\Delta S_m(\Delta H)|$  was determined from the  $C_P(T, H)$  data using Eq. (1) as described above. In this case,  $\Delta H = 8$  T. Similarly, Eq. (3) was applied to the magnetization data of Fig. 5 and the same quantity,  $|\Delta S_m(\Delta H)|$ , was determined using  $|\Delta S_m(\Delta H)| = |\Delta S_m(H = 8\text{ T}) - \Delta S_m(H = 0.2\text{ T})|$  (note that  $H = 0.2$  T was the smallest field used). The data obtained from these two methods should agree, since entropy is an intrinsic property. Figure 6 shows the results.  $|\Delta S_m(\Delta H)|$  obtained from the two independent methods agrees very well for CoSb<sub>2</sub>O<sub>6</sub>, with the data for both methods of similar magnitude, near  $|\Delta S_m(8\text{ T})| \sim 2.7$  J/kg K. In the case of NiTa<sub>2</sub>O<sub>6</sub>, a significantly smaller effect of  $|\Delta S_m(8\text{ T})| \sim 0.7$  J/kg K is observed, and the two methods agree less well. The entropy change associated with  $H \parallel [001]$  is small for both samples, as expected. In some cases, multiple peaks occur in the  $|\Delta S_m(\Delta H)|$  data. This is associated with the small number of magnetic fields available for the analysis. Notable is the difference in the  $|\Delta S_m(\Delta H)|$  data for  $H \parallel [110]$  and  $H \parallel [001]$ . Rotating the sample between these two field directions at *constant* magnetic field would lead to  $|\Delta S| \sim 2.1$  J/kg K in the case of CoSb<sub>2</sub>O<sub>6</sub>.

Finally, to determine the temperature change  $\Delta T$  associated with a given magnetic field change  $\Delta H$ , the relation

$$\Delta T = - \int_{H_1}^{H_2} \left( \frac{T}{C_P(T, H)} \right) \left( \frac{\partial M}{\partial T} \right)_H dH \quad (4)$$

is used. The results are shown in Fig. 7. Data for  $H \parallel [110]$  were obtained by plotting the integrand of Eq. (4) for  $H = 0.2, 2, 4, 6,$  and  $8$  T, followed by numerical integration. Data for  $H \parallel [100]$  and  $H \parallel [001]$  were obtained using  $H = 0.2$  T and  $H = 8$  T data only; use of two magnetic fields underestimates  $\Delta T$  by about 7% compared to  $\Delta T$  obtained using 5 fields. Note that the  $\Delta T$  for CoSb<sub>2</sub>O<sub>6</sub> are all negative as would be expected from a peak shift to lower temperature due to increasing  $H$ . The maximum magnitude of  $\Delta T$  reaches  $\sim 1$  K for NiTa<sub>2</sub>O<sub>6</sub> and 3 K for CoSb<sub>2</sub>O<sub>6</sub>. As expected, there exists significant anisotropy between  $H \parallel [110]$  and  $[001]$ . In all cases, the change in temperature due to the application of field tends toward zero for temperatures above  $T_N$ , as would be expected.

## VII. CONCLUSIONS

Measurements of the magnetic susceptibility  $\chi$  and heat capacity  $C_P$  as functions of temperature and magnetic field  $H$  have been used to learn about the ordering of the

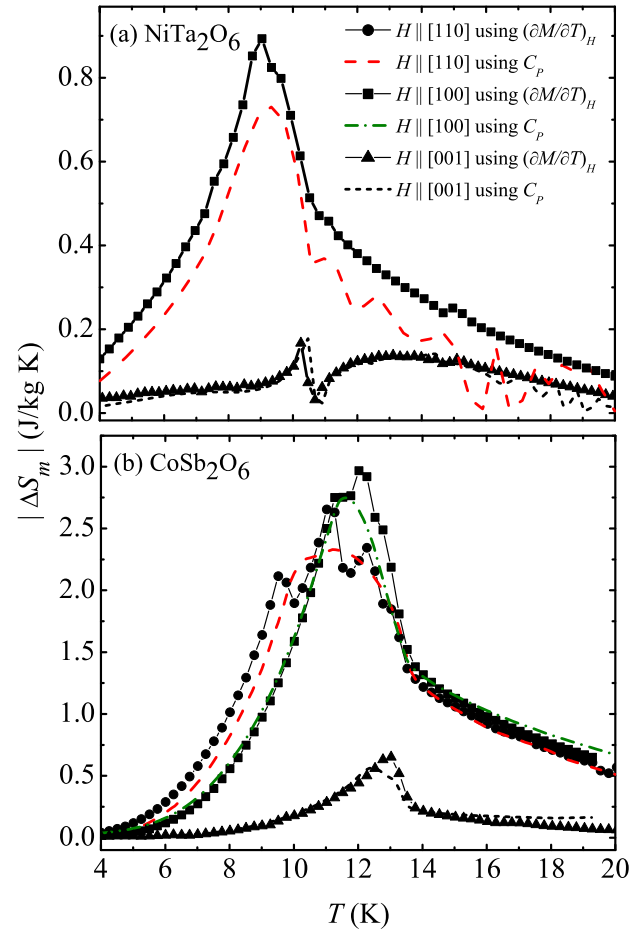


FIG. 6. (Color online) Change in magnetic entropy  $|\Delta S_m(8\text{ T})|$  obtained using Eq. (1) (red, green, and black dashed lines) and Eq. (3) (data points with lines) for (a) NiTa<sub>2</sub>O<sub>6</sub> and (b) CoSb<sub>2</sub>O<sub>6</sub>.

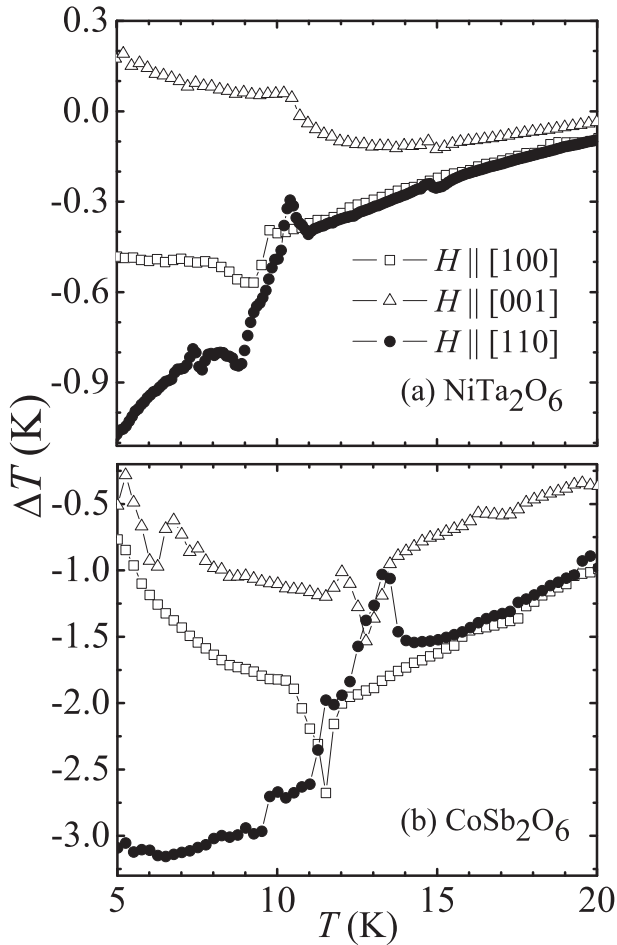


FIG. 7. Change in temperature  $\Delta T$  realized through a change in magnetic field  $H$  determined with Eq. (4). Data for  $H \parallel [110]$  (filled circles),  $H \parallel [100]$  (open squares), and  $H \parallel [001]$  (open triangles) are shown for (a)  $\text{NiTa}_2\text{O}_6$  and (b)  $\text{CoSb}_2\text{O}_6$ .

antiferromagnetic moments for  $\text{CuSb}_2\text{O}_6$ ,  $\text{NiTa}_2\text{O}_6$ , and  $\text{CoSb}_2\text{O}_6$ . The magnetic moments for all three compounds lie parallel to the  $a$ - $b$  plane. Within the plane, the analysis indicates that the magnetic moments of  $\text{CuSb}_2\text{O}_6$  lie nearly parallel to the  $[010]$  direction, in agreement with two determinations from single-crystal neutron diffraction [7,28]. For  $\text{NiTa}_2\text{O}_6$  and  $\text{CoSb}_2\text{O}_6$ , a model with the antiparallel moments along  $[110]$  at  $z = 0$  and the adjacent layer, at  $z = 1/2$ , with antiparallel moments along  $[1\bar{1}0]$ , is suggested by our experimental results; this is referred to as the two-sublattice model (sometimes called the orthogonal model) [11], and it is consistent with band structure calculations [15].

Proper determination of the antiferromagnetic structures is an important step toward understanding the physical properties of these compounds. The extremely weak coupling between the sublattices in the quasi-1D magnetic solids  $\text{NiTa}_2\text{O}_6$  and  $\text{CoSb}_2\text{O}_6$  leads to the presence of two antiferromagnetic transitions when the magnetic field  $H$  is parallel to the

quasi-1D chains of one lattice and perpendicular to the those of the second. This is associated with a mixture of Néel, dimer, and spin-liquid states at  $T_N$ , the mixture of which is sensitive to magnetic field and its direction within the plane. The typical magnetic field required to disrupt the magnetic ordering along the chain is about 2 T, which corresponds to an energy on the order of 0.2 meV.

The observations herein support an interpretation that the magnetic ordering in  $\text{NiTa}_2\text{O}_6$  and  $\text{CoSb}_2\text{O}_6$  is low-dimensional in nature, with extremely weak coupling along the  $c$  direction. Since magnetic field easily rotates the magnetic moments from their planar ordered arrangements in the sublattice, the antiferromagnetic coupling between neighboring 1D chains in each sublattice also appears to be weak. This agrees with band structure calculations [15], where the magnetic exchange between Ni ions of neighboring 1D chains is about an order of magnitude weaker than the exchange between Ni ions within the 1D chains. Long-range magnetic order is not expected for purely 1D systems. Therefore, the weak coupling perpendicular to the quasi-1D chains is the likely source of the 3D ordering that is observed [20–22]. These considerations provide further support for the assertion that  $\text{NiTa}_2\text{O}_6$  and  $\text{CoSb}_2\text{O}_6$  can be considered quasi-1D antiferromagnets.

The results presented herein reveal that the magnetic order of  $\text{NiTa}_2\text{O}_6$  and  $\text{CoSb}_2\text{O}_6$  can be easily manipulated with magnetic field. This leads to a magnetocaloric effect that is highly anisotropic by virtue of the quasi-1D nature of the antiferromagnetism; the magnetocaloric effect is modest in magnitude. The anisotropy indicates that rotation of  $\text{NiTa}_2\text{O}_6$  and  $\text{CoSb}_2\text{O}_6$  single crystals in magnetic field would cause them to change temperature. While anisotropy in the MCE of conventional antiferromagnets has been reported in a few cases [31,32], it has not been widely studied [40] and we are unaware of previous investigations of the MCE's anisotropy in quasi-1D antiferromagnets. The MCE reported herein differs from that observed [33] and theoretically studied [34–37] for low-dimensional quantum-spin systems, where saturation to a fully-polarized magnetic system is responsible. In the case of  $\text{NiTa}_2\text{O}_6$  and  $\text{CoSb}_2\text{O}_6$ , the MCE is associated with the unusual antiferromagnetic ordering of the quasi-1D spin system, and the disruption of that ordering through the application of magnetic field. That is, the orientation of each sublattice with regard to  $H$  as well as the poor magnetic coupling between adjacent sublattices and quasi-1D chains are responsible for the MCE. This unique aspect to the magnetic lattice, as well as the mixture of Néel, dimer, and spin-liquid states at  $T_N$ , is behind the anisotropic sensitivity of the magnetic ordering to magnetic field applied within the  $a$ - $b$  plane.

#### ACKNOWLEDGMENTS

This work was supported by the National Science Foundation under Contract No. DMR-0907036, CNPq-Brazil under Grant No. 237050/2012-9, and Montana State University. We gratefully acknowledge discussions with J. L. Cohn, M. G. Smith, and Anton Vorontsov.

[1] M. Takano and T. Takada, *Mater. Res. Bull.* **5**, 449 (1970).

[2] R. K. Kremer, J. E. Greedan, E. Gmelin, W. Dai, M. A. White,

S. M. Eicher, and K. J. Lushington, *J. Phys. Colloques (Paris)* **49**, C8-1495 (1988).

- [3] A. Nakua, H. Yun, J. N. Reimers, J. E. Greedan, and C. V. Stager, *J. Solid State Chem.* **91**, 105 (1991).
- [4] E. Ramos, M. L. Veiga, F. Fernández, and R. Saez-Puche, *J. Solid State Chem.* **91**, 113 (1991).
- [5] E. Ramos, F. Fernández, A. Jerez, C. Pico, J. Rodriguez-Carvajal, R. Saez-Puche, and M. L. Veiga, *Mater. Res. Bull.* **27**, 1041 (1992).
- [6] L. I. Zawislak, G. L. F. Fraga, J. B. Marimon da Cunha, D. Schmitt, A. S. Carrigo, and C. A. dos Santos, *J. Phys.: Condens. Matter* **9**, 2295 (1997).
- [7] M. Kato, K. Kajimoto, K. Yoshimura, K. Kosuge, M. Nishi, and K. Kakurai, *J. Phys. Soc. Jpn.* **71**, 187 (2002).
- [8] J. N. Reimers, J. E. Greedan, C. V. Stager, and R. Kremer, *J. Solid State Chem.* **83**, 20 (1989).
- [9] A. Rebello, M. G. Smith, J. J. Neumeier, B. D. White, and Y.-K. Yu, *Phys. Rev. B* **87**, 224427 (2013).
- [10] R. K. Kremer and J. E. Greedan, *J. Solid State Chem.* **73**, 579 (1988).
- [11] A. M. Nakua and J. E. Greedan, *J. Solid State Chem.* **118**, 199 (1995).
- [12] B. J. Gibson, R. K. Kremer, A. V. Prokofiev, W. Assmus, and B. Ouladdiaf, *J. Magn. Magn. Mater.* **272-276**, 927 (2004).
- [13] A. B. Christian, A. Rebello, M. G. Smith, and J. J. Neumeier (unpublished).
- [14] D. Kasinathan, K. Koepf, and H. Rosner, *Phys. Rev. Lett.* **100**, 237202 (2008).
- [15] J. M. Law, H.-J. Koo, M.-H. Whangbo, E. Brücher, V. Pomjakushin, and R. K. Kremer, *Phys. Rev. B* **89**, 014423 (2014).
- [16] F. D. M. Haldane, *J. Phys. C: Solid State* **14**, 2585 (1981).
- [17] E. Pytte, *Phys. Rev. B* **10**, 2039 (1974); **10**, 4637 (1974).
- [18] M. C. Cross and D. S. Fisher, *Phys. Rev. B* **19**, 402 (1979).
- [19] F. D. M. Haldane, *Phys. Rev. B* **25**, 4925 (1982).
- [20] H. J. Schulz, *Phys. Rev. Lett.* **77**, 2790 (1996).
- [21] Z. Wang, *Phys. Rev. Lett.* **78**, 126 (1997).
- [22] T. Giamarchi, *Quantum Physics in One Dimension* (Clarendon Press, Oxford, 2003), p. 188.
- [23] M. Kenzelmann, R. Coldea, D. A. Tennant, D. Visser, M. Hofmann, P. Smeibidl, and Z. Tylczynski, *Phys. Rev. B* **65**, 144432 (2002).
- [24] D. V. Dmitriev and V. Ya. Krivnov, *JETP Lett.* **80**, 303 (2004); *Phys. Rev. B* **70**, 144414 (2004).
- [25] J. Kurmann, G. Müller, H. Thomas, M. W. Puga, and H. Beck, *J. Appl. Phys.* **52**, 1968 (1981); J. Kurmann, H. Thomas, and G. Müller, *Physica A* **112**, 235 (1982).
- [26] H. Ehrenberg, G. Wltschek, J. Rodriguez-Carvajal, and T. Vogt, *J. Magn. Magn. Mater.* **184**, 111 (1998).
- [27] E.-O. Giere, A. Brahim, H. J. Deiseroth, and D. Reinen, *J. Solid State Chem.* **131**, 263 (1997).
- [28] E. M. da Silva Wheeler, Ph.D. thesis, Oxford University, 2007.
- [29]  $J_{\perp}$  used here is the strongest interlayer coupling value, which is along the  $[\frac{1}{2}\frac{1}{2}\frac{1}{2}]$  direction.
- [30] S. M. Eicher, J. E. Greedan, and K. J. Lushington, *J. Solid State Chem.* **62**, 220 (1986).
- [31] S. A. Nikitin, K. P. Skokov, Yu. S. Koshkid'ko, Yu. G. Pastushenkov, and T. I. Ivanova, *Phys. Rev. Lett.* **105**, 137205 (2010).
- [32] R. D. dos Reis, L. M. da Silva, A. O. dos Santos, A. M. N. Medina, L. P. Cardoso, and F. C. G. Gandra, *J. Alloys Compd.* **582**, 461 (2014).
- [33] B. Wolf, Y. Tsui, D. Jasiwal-Nagar, U. Tutsch, A. Honecker, K. Remović-Langer, G. Hofmann, A. Prokofiev, W. Assmus, G. Donath, and M. Lang, *Proc. Natl. Acad. Sci. USA* **108**, 6862 (2011).
- [34] M. E. Zhitomirsky and A. Honecker, *J. Stat. Mech.: Theor. Exp.* (2004) P07012.
- [35] A. Honecker and S. Wessel, *Physica B* **378-380**, 1098 (2006).
- [36] O. Derzhko and J. Richter, *Eur. Phys. J. B* **52**, 23 (2006).
- [37] R. Jafari, *Eur. Phys. J. B* **85**, 167 (2012).
- [38] A. V. Prokofiev, F. Ritter, W. Assmus, B. J. Gibson, and R. K. Kremer, *J. Cryst. Growth* **247**, 457 (2003).
- [39] C. Kittel, *Introduction to Solid State Physics*, 7th ed. (Wiley, New York, 1996), p. 465.
- [40] K. A. Gschneidner, Jr., V. K. Pecharsky, and A. O. Tsokol, *Rep. Prog. Phys.* **68**, 1479 (2005).